

Semiring Primitives for Sparse Neighborhood Methods on the GPU

Corey J. Nolet

cjnolet@gmail.com

NVIDIA

Univ. of MD, Baltimore County
USA

Joe Eaton

featon@nvidia.com

NVIDIA

USA

Divye Gala

dgala@nvidia.com

NVIDIA

USA

Edward Raff

raff_edward@bah.com

Booz Allen Hamilton

Univ. of MD, Baltimore County
USA

Brad Rees

brees@nvidia.com

NVIDIA

USA

John Zedlewski

jzedlewski@nvidia.com

NVIDIA

USA

Tim Oates

james_oates@umbc.edu

Univ. of MD, Baltimore County

USA

ABSTRACT

High-performance primitives for mathematical operations on sparse vectors must deal with the challenges of skewed degree distributions and limits on memory consumption that are typically not issues in dense operations. We demonstrate that a sparse semiring primitive can be flexible enough to support a wide range of critical distance measures while maintaining performance and memory efficiency on the GPU. We further show that this primitive is a foundational component for enabling many neighborhood-based information retrieval and machine learning algorithms to accept sparse input. To our knowledge, this is the first work aiming to unify the computation of several critical distance measures on the GPU under a single flexible design paradigm and we hope that it provides a good baseline for future research in this area. Our implementation is fully open source and publicly available at <https://github.com/rapidsai/cuml>.

CCS CONCEPTS

• GPGPU Computing; • Machine Learning; • Nearest Neighbors; • Distance Metrics;

KEYWORDS

nearest neighbors, distance metric, GPU, semiring

1 INTRODUCTION

Machine learning applications most often deal with sets of vectors in high-dimensions where each dimension corresponds to an individual feature or observation. Sparse formats are often used in machine learning algorithms to represent bipartite graphs, and an important step in neighborhood-based machine learning methods is the computation and representation of affinities, or neighborhoods, between the vectors within the bipartite graph. For example, the brute-force k-nearest neighbors and epsilon neighbors methods compute neighborhoods around each vector by first performing an exhaustive computation of distances between all the vectors in some topological space. The machine learning algorithms which

rely on pairwise distances span the spectrum of categories from dimensionality reduction to clustering and statistical analysis to classification and regression. Pairwise distances are also essential to any method that uses the *representer theorem* [43] to harness reproducing kernel Hilbert spaces (RKHS) [7, 12, 44, 46].

The *MapReduce* [17] paradigm is widespread in distributed and parallel computing environments, in part because it inserts a layer of abstraction between the developer and the hardware, enabling the developer to think about scale in terms of primitive operations and trusting the underlying execution framework to make efficient use of the resources available. This benefits increased performance and scale, but designing algorithms with a unified representation also further promotes reuse and accelerates time to market.

General-purpose GPU computing (GPGPU) has grown in significance in recent years as a means of accelerating compute-heavy workloads. More recently, libraries like Pytorch, Tensorflow, and RAPIDS have been putting this power in the hands of developers, analysts, and even domain experts, affording them the benefit of GPU acceleration by interacting with familiar Python APIs. GPUs work best when memory access patterns are contiguous and instructions are kept as uniform as possible. This makes it especially appealing for applications which can be expressed using dense linear algebra but poses challenges for linear algebra on very sparse datasets [24] where the distribution of nonzeros are often very skewed and emit small-world or power-law characteristics.

Semirings provide a useful paradigm for defining and computing inner product spaces in linear algebra using two operations, as in the *MapReduce* [20, 33] paradigm where a *product()* function is used to define a mapping between point-wise corresponding elements of vectors and a *sum()* function is used to reduce the products into a scalar. Using semirings to implement algorithms with sparse linear algebra on GPUs is an active area of research [21] and has been widely studied for helping to consolidate both the representation and execution of operations on graphs and probabilistic graphical models. In this paper, we show that semirings can be used for sparse neighborhood methods in machine learning, extending the

benefits to all algorithms capable of using them, which we cover briefly in the next section. We define semirings more formally in subsection 4.2 but use the more general description above to navigate the benefits and related work in the following section.

2 RELATED WORK

2.1 Sparse matrix multiplication

The task of efficient and performant sparse matrix multiplication is an active area of research, with implementations spanning the spectrum of scientific computing. In high performance computing environments, these solutions are designed around both hardware and software constraints [10, 22–24, 28], often making use of specialized hardware capabilities and optimizing for specific sparsity patterns, an unfortunate side-effect that can reduce their potential for reuse. What complicates this further are the number of different optimized variants of sparse matrix multiplication available in open source libraries, each using different concurrency patterns and available memory to provide speedups based on either supported sparse formats or the assumed density of either the inputs or the outputs [33, 45].

cuSPARSE [35] is a popular library that provides highly optimized generalized sparse linear algebra routines. It provides a sparse-matrix sparse-matrix multiply but it fixes the inner product to the dot product semiring (e.g. *sum()* is addition and *product()* is multiplication), which requires the user to manually transpose the right side of the input, B , and only produces sparse output. The last detail is critical to the memory footprint, as the outputs for most pairwise distances are inherently dense and, while this is not always assumed to be the case with a simple dot product semiring, we show in section 7 that storing these outputs in sparse form can lead to wasted memory in practice. While the cuSPARSE *csrgemm()* is a core building-block of recent work in GPU-accelerated sparse k-nearest neighbors [56], the additional memory required to construct the transposition of B , as well as the aforementioned conversion of the sparse output to dense form for computing even the basic Euclidean distance, has a significant impact on scale. Further, since the *csrgemm()* and *spgemm* are not capable of computing inner products in any semiring other than the dot product, cuSPARSE leaves the burden of computing distances, like Manhattan distance which can't be derived from the dot product, completely to the user. More extensive research into generalized sparse-matrix sparse-matrix (spsm) and sparse-matrix sparse-vector multiply (spsv) algorithms uncovers similar patterns- either solutions are optimized to very specific use-cases which are orthogonal to the general computation of pairwise distances, or are generalized to cover the widest range of applications, making them less flexible and/or efficient.

Better able to make use of critical optimizations inherent in their dense counterparts, block compressed sparse formats have become widely popular for representing sparse data [53], in part because they can improve load balancing by grouping nonzeros into fixed-sized tiles and scheduling the tiles more uniformly across the processing cores. Enabling sparse formats to be processed more similar to their dense counterparts allows the use of specialized hardware optimizations such as tensor cores. While we do hope to someday support block-sparse formats, it is most often assumed that users will be calling code that invokes our primitive with matrices

in the standard compressed sparse row (CSR) format [50] (which we describe in section 3) and so a conversion would be necessary in order to use a blocked format.

2.2 Semirings

A common issue for large-scale sparse problems in high-performance single-instruction multiple-data (SIMD) environments, like the GPU, is load balancing in order to keep the processing units constantly moving forward. As we will show in Section 5, the imbalanced load and resource requirements for a simple and straightforward naive semiring implementation, capable of computing distances like Manhattan, suffers from thread divergence within warps, highly uncoalesced global memory accesses, and resource requirements which are unrealistic in many real-world datasets.

In order to integrate into an end-to-end data science or scientific computing workflow, such as in the PyData or RAPIDS [41] ecosystems, an efficient implementation of a primitive for computing pairwise distances on sparse datasets should ideally preserve as many of the following characteristics as possible:

- (1) maintain uniformity of intra-warp instruction processing
- (2) coalesce both reads from and writes to global memory
- (3) process data inputs without transposition or copying
- (4) use as little memory as necessary
- (5) enable semirings in addition to the simple dot product

Consolidating seemingly disparate concepts into a lightweight, terse, and abstract set of building-blocks can increase flexibility and promote reuse [27]. This especially benefits fields which require non-trivial and highly-optimized implementations where the design complexities and costs are high, the basic linear-algebra subroutines (BLAS) API and GPU-accelerated computing being common examples. Semirings provide the efficiency and flexibility to enable algorithms in which the representation and assumptions of the typical BLAS API for dense linear algebra comes up short [33]. NIST published a sparse BLAS standard back in 2001 [19] and cuSPARSE is one of the most sophisticated implementations of the sparse BLAS standard that has been built on the GPU, however as mentioned above, its multiplication routines fix the inner product to the dot product. GraphBLAS [15] provides a set of primitives, along with an API, for using semiring algebras to implement graph algorithms. The GraphBLAST [52] and SuiteSparse [16] libraries provide implementations of the GraphBLAS that also include GPU-accelerated primitives.

The use of semirings in graph theory dates back to the early 1970s [42], when "good old-fashioned artificial intelligence", or *Symbolic AI*, was a dominant paradigm in research. Semirings have also been used for some time to implement more modern machine learning methods [11], with the more recent invention of semiring programming attempting to further consolidate these concepts under a single framework and set of symbolic routines. Semirings can be a useful building-block for probabilistic models, such as Bayesian networks [49] and the use of Tropical semiring in Markov networks [26]. The Tropical semiring is also being used to implement sparse non-negative matrix factorizations [38].

Composing algorithms with semiring primitives has an additional benefit of decoupling their representation from their execution, adding a layer of indirection so algorithms can be scaled in

both highly parallel and even highly distributed environments in a straightforward manner. This is another very important similarity to MapReduce but is also not unlike the more recent examples of Tensorflow [3] or PyTorch [40].

While a comprehensive and generalized collection of building blocks for implementing semirings is within scope for both SuiteSparse and GraphBLAST, the scope of our work is much more narrow. In this paper, we provide an analysis of how semiring algebras can expand the scope of existing semiring libraries to include sparse neighborhood methods in machine learning and provide an initial set of GPU-accelerated primitives to enable them.

2.3 Neighborhood Methods

An optimized semiring primitive has the potential to have significant impact on neighborhood methods in data mining and machine learning applications [18]. Core to many neighborhood methods is the ability to sparsify a fully-connected graph of pairwise distances into an adjacency matrix of connectivities by using only the k-nearest or epsilon neighborhoods around each vertex. The use of cuSPARSE for the dot product semiring, an approach which has been taken by other k-nearest neighbors implementations on the GPU [56], severely limits flexibility by constraining any supported distances to those which can be derived from the dot product. Further, when integrating this implementation into an end-to-end data science platform, such as Scikit-learn, the inputs are assumed to be in their original non-transposed format and so a memory copy would be required to use cuSPARSE. This is compounded even further when the entire matrix of $m * n$ pairwise distances needs to fit into the memory space of the GPU. Our k-nearest neighbors solution computes only a single tile of the pairwise distance matrix at a time and so requires only a single tile fit into GPU memory in addition to the inputs. Similarly to [56], we perform a k-selection on the resulting pairwise distances but we avoid additional sorting and accesses to global memory using the heap-based variant of Batcher's bitonic sorting network from [29].

Any positive semi-definite pairwise distance matrix can utilize RKHS and many of the commonly used kernel functions can be computed with embarrassingly parallel computations over an existing pairwise distance matrix. The capability to compute pairwise distances, k-nearest neighbors, and epsilon neighborhoods allows our primitive to enable sparse inputs into many dimensionality reduction and manifold learning algorithms including Kernel PCA, Locally Linear Embeddings (LLE), Local Tangent Space Alignment, Spectral Embeddings, Multidimensional Scaling (MDS), Hessian Eigenmaps, IsoMap, Uniform Manifold Approximation and Projection (UMAP), and t-Distributed Stochastic Neighborhood Embeddings (t-SNE). Embeddings are often used for analysis, feature engineering, visualization, and improving downstream classification results and they have become a very active area of research. Many of these algorithms share so many similarities that a library has been written to consolidate them into a manageable and flexible set of expressive primitives [4].

In addition to embedding techniques, our primitive enables many important clustering and community detection algorithms, including k-means, k-medoids, mean-shift clustering, Louvain, Leiden,

OPTICS, DBSCAN / HDBSCAN, Single- and complete-linkage agglomerative clustering, and Laplacian eigenmaps. Gaussian processes [31] utilize RKHS to construct priors from covariance matrices and the impact of neighborhood methods are even present in classification and regression tasks. In addition to k-nearest neighbors, when coupled with a voting or label aggregation primitive, support vector machines (SVM) and kernel ridge regression are examples of using RKHS to learn non-linear decision boundaries.

3 SPARSE DATA

Our application accepts matrices in the compressed sparse row (CSR) format, which uses 3 arrays to represent only the nonzero elements. Two of these arrays store the column indices and values and require the entire list of nonzero elements. These arrays are required to be sorted by the row so that the third array only need store the cumulative sum of index offsets into them, one offset per row. Ideally, a memory-efficient solution would be able to process the CSR format directly, without creating additional indexing, but this can also create challenges to load-balancing [51]. The coordinate format (COO) is very similar to the CSR format. As shown in Figure 1, the only difference from CSR is that the row index array is expanded to contain all of the rows for the nonzero values. Our implementation uses this expanded row index array to help balance load.

For data to be efficiently represented in sparse form, the ratio of the number of nonzeros to the number of potential elements in the dense representation needs to be significantly small. While there is no universally accepted threshold of zeros to nonzeros that would constitute using a sparse format, the CSR representation of a sparse matrix at 50% density would have a larger memory footprint, because of the additional CSR indptr array, than just storing the data in dense form. Similarly, a COO matrix would take up the same amount of space at 33% density as it would in its sparse form.

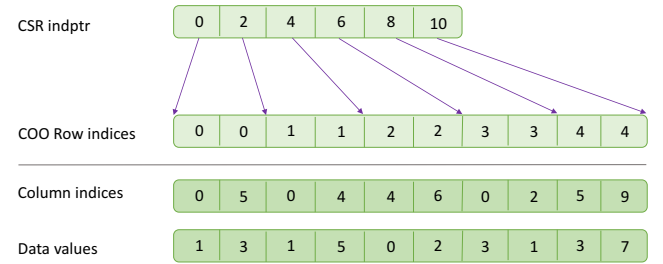


Figure 1: Example of our CSR index being used to index into a sorted COO index. [37]

Sparse data in machine learning applications is often used to represent either a connectivities matrix or bipartite graph, such as a doc-term matrix in natural language processing applications, a user-item matrix in recommender systems, or a cell-gene expressions matrix in single-cell and tertiary genomics analysis applications. Many machine learning algorithms that accept sparse data will compute a connectivities graph by sparsifying a fully-connected graph of pairwise distances using information about neighborhood

structure. While our implementation demonstrates reasonable performance with both connectivities and bipartite graphs, it is the latter which is of particular interest in the scope of this paper.

While degree distributions of rows in both of these graphs tend to vary widely depending on the individual application and dataset, they rarely have a completely uniform distribution, and will generally admit some amount of positive skew.

4 SEMIRINGS AND PAIRWISE DISTANCES

We formalize the concepts of semirings and distance measures in this section and describe building blocks required to implement several popular distance measures, often encountered in machine learning applications, into the semiring framework.

In machine learning applications, a distance measure is often performed on two row matrices containing data samples with columns that represent some number of observations, or features. In this paper, we will refer to these two matrices as A and B in upper-case where $A \in \mathbb{R}^{m \times k}$, and $B \in \mathbb{R}^{n \times k}$ and a single vector as a and b in lowercase where $a \in \mathbb{R}^k$ or $b \in \mathbb{R}^k$. As we show in this section, the core of computing pairwise distances between A and B is a matrix multiplication AB^T in a topological space equipped with an inner product semiring that defines distances between vectors. When this inner product is defined to be the dot product semiring, the topological space defines the standard matrix multiply but we can capture many other core distances in machine learning applications by simply redefining the inner product semiring.

While some distance measures can make use of the simple dot product semiring from matrix-matrix multiplication routines, we show that a more comprehensive package for computing pairwise distances requires more flexibility in terms of the arithmetic operations supported. Further, the explicit transposition of B which is required in routines such as the cuSPARSE `csrgemm()` requires a full copy of B , since no elements can be shared between the original and transposed versions in the CSR data format. This has a negative impact on scalability in memory-constrained environments such as GPUs.

4.1 Distances

Sparse matrix-matrix multiplication with a standard dot product semiring is most performant in cases where only the intersection is needed between pairs of corresponding nonzero columns in each vector. Because a standard multiplication between two terms has an identity of 1 and multiplicative annihilation (e.g. $a_i * 0 = 0$), the dot product semiring between two vectors can be computed efficiently by iterating over the nonzero columns of one vector and only computing the product of the corresponding nonzero columns of the other vector. Many distances can make use of this property, as shown in table 1 in the distances that can be represented with an expansion function.

$$d(a, b) \geq 0 \quad (1)$$

$$d(a, b) = d(b, a) \quad (2)$$

$$d(a, c) \leq d(a, b) + d(b, c) \quad (3)$$

$$(\sum_i^k |a_i - b_i|^p)^{1/p} \quad (4)$$

For a distance to define a metric space, it must follow the three properties in Equations 1, 2, and 3. Several metrics, including Chebyshev, Manhattan, and Euclidean, are derived from the generalized Minkowski formula in Equation 4 where p defines a degree. The absolute value in this equation defines a commutative semiring which requires commutativity in the difference of each vector dimension. Euclidean distance is equivalent to Minkowski with a degree of 2 ($(\sum_i^k |a_i - b_i|^2)^{1/2}$). Because the square of a number is always positive, this equation can be expanded to $(a - b)^p$ for all even degrees and still preserve the absolute value, such as $(a - b)^2 = a^2 - 2\langle a, b \rangle + b^2$ in the case of Euclidean distance. While numerical instabilities can arise from cancellations in these expanded equations, we will show in section 4.2 that the expanded form is often preferred in sparse algebras, when distances can make use of it, because it requires less computations than the exhaustive evaluation over the nonzeros of k . By example, the distances which don't have an expanded form, such as Manhattan (Minkowski with degree 1) and Chebyshev (Minkowski with degree \max) distance, are often non-annihilating (e.g. $x * 0 = x$) and require computation over the full union of nonzero columns from both vectors in order to preserve commutativity.

4.2 Semirings

A *monoid* is a semigroup containing an associative binary relation, such as addition (\oplus), and an identity element (id_{\oplus}). A *semiring* [42], denoted $(S, \mathbb{R}, \{\oplus, id_{\oplus}\}, \{\otimes, id_{\otimes}\})$, is a tuple endowed with a domain along with additive (\oplus) and multiplicative (\otimes) monoids where

- (1) \oplus is commutative, distributive, and has an identity element 0
- (2) \otimes distributes over \oplus

Some formal definitions of semirings require that $id_{\otimes} = 1$. Given two sparse vectors $a, b \in \mathbb{R}^k$, a semiring with $(S, \mathbb{R}, \{\oplus, 0\}, \{\otimes, 1\})$ and $annihilator_{\otimes} = 0$ has the effect of only requiring \otimes be computed on columns that are both nonzero (e.g. $nonzeros(a) \cap nonzeros(b)$). These rules are often relaxed in practice, for example in tropical semirings in Equation 5, which can solve dynamic programming problems such as the Viterbi algorithm. An *annihilator* is an input that will always cause a monoid to evaluate to 0 and the multiplicative annihilator ($annihilator_{\otimes}$) is often assumed to be id_{\oplus} . A monoid is non-annihilating when it does not have a defined annihilator. When an expanded form is not possible or efficient, \otimes also must be commutative in metric spaces, and thus must be non-annihilating and $id_{\otimes} = 0$.

$$(S, \mathbb{R} \cup \{+\infty\}, \{min, +\infty\}, \{+, 0\}) \quad (5)$$

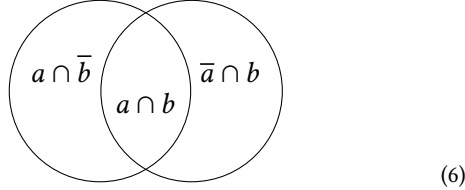
Table 1 uses semirings to construct several commonly used distances in machine learning applications. When an expanded form is possible, an expansion function can be performed as an element-wise operation on a simple pairwise dot product semiring with arrays of row-vector norms. While most of the expanded form distances can directly use the dot product semiring, KL-divergence

directly replaces the \otimes with $a_i \log(a_i/b_i)$ and makes no further assumption of symmetry. A non-annihilating \otimes is required for all unexpanded distance measures where $id_{\otimes} = 0$ and special care must be taken to ensure it is applied to the full union of the non-zero columns of corresponding elements from each pair of vectors.

As mentioned in the previous section, the Euclidean distance can be expanded to $\|A\| - 2\langle AB^T \rangle + \|B\|$. This equation can be decomposed into individual L2 norms and a matrix product and an element-wise expansion function executed in parallel over the individual dot products from the matrix product to combine the parts into a single distance. In the case of Euclidean distance, this expansion function over vector dot products A_i, B_j would become $\|A\|_i + 2\langle A_i, B_j \rangle - \|B\|_j$.

The $annihilator_{\otimes}$ and id_{\otimes} determine the number of times the \otimes monoid must be applied during the computation of pairwise distances. When $annihilator_{\otimes} = id_{\oplus}$, then $\otimes(a_i, 0) = 0$ and $\otimes(0, b_i) = 0$ so \otimes can be applied only to the intersection of columns. When $annihilator_{\otimes}$ is undefined and $id_{\otimes} = 0$, then \otimes must be applied exhaustively over the union of columns because $\otimes(a_i, 0) = a_i$ and $\otimes(0, b_i) = b_i$.

A union between two sets can be decomposed into an intersection between the two sets, along with the union of the symmetric differences between them. These are shown in Equation 7, where a complement is denoted with a $\bar{}$. The nonzero columns of two sparse vectors can be used as sets a and b in this equation and the sparse matrix multiply with an ordinary dot product only requires the application of $product()$ across $a \cap b$.



$$a \cup b = \{a \cap b\} \cup \{\bar{a} \cap b\} \cup \{a \cap \bar{b}\} \quad (7)$$

A common approach to implementing sparse matrix multiply is to iterate over the nonzeros from b in order to lookup and compute the intersection with the nonzeros from a . This design will also implicitly compute the symmetric difference between either of the two sets of nonzeros, $a \cap \bar{b}$ or $\bar{a} \cap b$, depending on which vector is chosen in the iteration over nonzeros. To compute a full union, the remaining set difference can be computed in a second pass of the matrix multiply by looping over the nonzeros from the vector that remains. We will show in section 5 that we accomplish this efficiently in our implementation in two passes- one pass to compute the first two terms and another pass to compute the third term. Expanded distances only need the first pass.

Existing semiring implementations currently require that the id_{\oplus} be used as $annihilator_{\otimes}$. For example, the GraphBLAS library enables the re-interpretation of the zeroth element, but this is necessary to define the identity of the \oplus monoid.

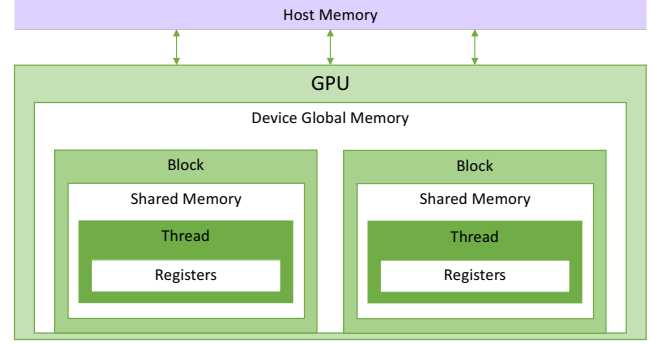


Figure 2: The GPU memory model [37]

5 GPU ARCHITECTURE

The largest GPUs today contain hundreds of hardware processing cores called streaming multiprocessors (SM) which execute groups of threads called warps. Each warp can process a single instruction at a time in parallel using a paradigm called single-instruction multiple data (SIMD). It's important that threads within a warp minimize conditional branching that will cause the threads to wait for each branch to complete before proceeding. This is called thread divergence, and can severely limit effective parallel execution. On the Volta and Ampere architectures, each SM can track the progress of up to 64 warps concurrently [47], and rapidly switch between them to fully utilize the SM. Each SM has a set of registers available which allows warps to perform collective operations, such as reductions. Warps can be grouped into blocks and a small amount of memory can be shared across the threads and warps.

Global, or device, memory can be accessed by all of the SMs in the GPU. Accesses to contiguous device memory locations within a warp can be coalesced into a single blocked transaction so long as the accesses are performed in the same operation. In SIMD architectures, uniform patterns can be critical to performance unless latencies from non-uniform processing, such as uncoalesced memory accesses, can be hidden with increased parallelism.

Registers provide the fastest storage, and it's generally preferable to perform reductions and arithmetic as intra-warp collective operations where possible. Intra-block shared memory is also generally preferred over global memory when a problem can be made small enough to benefit. However, contiguous locations of shared memory are partitioned across contiguous banks and any accesses to different addresses in the same bank by the same warp will create a bank conflict and be serialized within the warp, causing the threads to diverge.

6 GPU-ACCELERATED SEMIRINGS

In this section, we discuss some naive designs and the inefficiencies that led to the construction of our final design. Our goal was to preserve as many of the ideal design characteristics from section 2 as possible but we found a need to accept trade offs during implementation.

Distance	Formula	\otimes	Norm	Expansion
Correlation	$1 - \frac{\sum_{i=0}^k (x_i - \bar{x})(y_i - \bar{y})}{\sqrt{\sum_{i=0}^k x_i - \bar{x}^2} \sqrt{\sum_{i=0}^k y_i - \bar{y}^2}}$		μ, δ	$1 - \frac{\langle x \cdot y \rangle - \mu_x \mu_y}{\delta_x \delta_y}$
Cosine	$\frac{\sum_{i=0}^k x_i y_i}{\sqrt{\sum_{i=0}^k x_i^2} \sqrt{\sum_{i=0}^k y_i^2}}$		L_2	$1 - \frac{\langle x \cdot y \rangle}{\ x\ _2^2 \ y\ _2^2}$
Dice-Sorensen	$\frac{2 \sum_{i=0}^k x_i y_i }{(\sum_{i=0}^k x_i)^2 + (\sum_{i=0}^k y_i)^2}$		L_0	$\frac{2\langle x \cdot y \rangle}{\ x\ ^2 + \ y\ ^2}$
Dot Product	$\sum_{i=0}^k x_i y_i$	$\{*, 1\}$		$\langle x \cdot y \rangle$
Euclidean	$\sqrt{\sum_{i=0}^k x_i - y_i ^2}$	$\{ x - y ^2, 0\}$	L_2	$\ x\ _2^2 - 2 \langle x \cdot y \rangle + \ y\ _2^2$
Canberra	$\sum_{i=0}^k \frac{ x_i - y_i }{ x_i + y_i }$		$\{\frac{ x - y }{ x + y }, 0\}$	
Chebyshev	$\sum_{i=0}^k \max(x_i - y_i)$		$\{\max(x - y), 0\}$	
Hamming	$\frac{\sum_{i=0}^k x_i \neq y_i}{k}$		$\{x \neq y, 0\}$	
Hellinger	$\frac{1}{\sqrt{2}} \sqrt{\sum_{i=0}^k (\sqrt{x_i} - \sqrt{y_i})^2}$			$1 - \sqrt{\langle \sqrt{x} \cdot \sqrt{y} \rangle}$
Jaccard	$\frac{\sum_{i=0}^k x_i y_i}{(\sum_{i=0}^k x_i^2 + \sum_{i=0}^k y_i^2 - \sum_{i=0}^k x_i y_i)}$		L_0	$1 - \frac{\langle x \cdot y \rangle}{(\ x\ + \ y\ - \langle x \cdot y \rangle)}$
Jensen-Shannon	$\sqrt{\frac{\sum_{i=0}^k x_i \log \frac{x_i}{\mu_i} + y_i \log \frac{y_i}{\mu_i}}{2}}$		$\{x \log \frac{x}{\mu} + y \log \frac{y}{\mu}, 0\}$	
KL-Divergence	$\sum_{i=0}^k x_i \log(\frac{x_i}{y_i})$		$\{x \log(\frac{x}{y}), 1\}$	$\langle x \cdot y \rangle$
Manhattan	$\sum_{i=0}^k x_i - y_i $		$\{ x - y , 0\}$	
Minkowski	$(\sum_{i=0}^k x_i - y_i ^p)^{1/p}$		$\{ x - y ^p, 0\}$	
Russel-Rao	$\frac{k - \sum_{i=0}^k x_i y_i}{k}$			$\frac{k - \langle x \cdot y \rangle}{k}$

Table 1: Common distances and their semirings. Any \otimes monoids where $id_{\otimes} = 0$ needs to be computed in unexpanded form. The expansion function and any potential norms are provided for distances that can be computed in the more efficient expanded form.

6.1 Full-Union CSR Designs

6.1.1 *Expand-Sort-Contract*. Initial implementations tried to minimize the memory footprint as much as possible by directly computing the output distances from the input CSR format. The CSR format requires columns to be sorted with respect to row and we initially attempted to use a modified variant of the *expand-sort-contract* [14] pattern on the nonzero columns from each pair of row vectors, $a, b \in \mathbb{R}^k$, concatenating the vectors together, sorting them, and applying the \otimes monoid on pairs of duplicate columns to *contract* the sorted array and invoking \otimes with the identity for all other columns. At the row-level of the output matrix, no computations would be able to be reused by subsequent pairs of vectors so we implemented this pattern on the GPU and mapped the nonzero columns and values for each row-vector pair to individual thread-blocks, *expanding* both vectors by concatenating them in shared memory, performing a sort-by-key, and compressing them in parallel. We attempted several efficient sorting algorithms on the GPU including the popular radix sort and bitonic sorting networks and, while the use of shared

memory in the sort step enabled coalesced reads from global memory for the nonzero columns and values, the sorting step dominated the performance of the algorithm. Another downside with this particular design is that both vectors need to fit in shared memory, requiring space for $2 * (nonzeros(a) + nonzeros(b))$ elements in order to fit both the columns and corresponding values at the same time. In addition to the need for $n * m$ blocks to be scheduled, the shared memory requirement became a severe limit to scale, which was further compounded by the shared memory size limiting the number of blocks that could be scheduled concurrently on each SM.

6.1.2 *Iterating Sorted Nonzeros*. Since columns will often be sorted within their respective rows in the CSR format, we removed the sort step from algorithm 1 by exhaustively iterating over the non-zeros of each $O(m * n)$ pair of vectors in parallel, one pair per thread, as shown in algorithm 2. We found that even when the neighboring threads processed rows of similar degree, the differing distributions of nonzeros within each row decreased the potential for coalesced

Input: $A_i, B_j, product_op, reduce_op$

Result: $C_{ij} = d(A_i, B_j)$

$smem[0..nnz_a_i - 1] = A_i;$

$smem[nnz_a_i..nnz_b_j - 1] = B_j;$

$sort(smem);$

$C_{ij} = reduce(smem, product_op, reduce_op);$

Algorithm 1: Semiring on CSR inputs using expand-sort-contract pattern, parallelized across threads in each block.

global memory accesses and created large thread divergences. Further, the exhaustive nature of this design, while it will guarantee the \otimes monoid is computed on the full union of nonzero columns, will end up performing many unnecessary computations when distances can be computed with the rules of a simple dot product semiring.

Input: $A_i, B_j, product_op, reduce_op$

Result: $C_{ij} = d(A_i, B_j)$

$startA = indptrA_i, endA = indptrA_{i+1};$

$startB = indptrB_j, endB = indptrB_{j+1};$

$i_colA = startA, i_colB = startB;$

while $i_colA < endA \parallel i_colB < endB$ **do**

$colA = i_colA < endA ? indices_{i_colA} : MAX_INT;$

$colB = i_colB < endB ? indices_{i_colB} : MAX_INT;$

$valueA = 0, valueB = 0;$

if $colA \leq colB$ **then**

$valueA = values_{A_colA++};$

end

if $colB \leq colA$ **then**

$valueB = values_{B_colB++};$

end

$v = product_op(valueA, valueB);$

$C_{ij} = reduce_op(C_{ij}, v);$

end

Algorithm 2: Semiring on CSR inputs. Each thread computes a single dot product.

We found marginal gains in performance by coalescing the reads of the vectors from A into shared memory and sharing it across all threads of each thread-block. We attempted to load balance this algorithm by maintaining arrays to look up row information for each column but this increased warp divergence from the overly complicated conditionals required to maintain state across threads and warp boundaries.

6.2 Load Balanced Hybrid CSR+COO

While the CSR format enables algorithms to be parallelized over threads for individual rows, we found that using a row index array in coordinate format (COO) for B enabled load balancing, coalescing the loads from each vector from A into shared memory, once per block, and threads of each block parallelizing the application of the semiring over nonzero elements of B . Since the columns in B are assumed to be sorted by their respective row, we use a segmented reduction by key within each warp, bounding the number of potential writes to global memory by the number of active

warps over each row of B . Our design extends the work of the COO sparse-matrix dense-vector multiplication described in [2] by storing the vectors from A in dense form in shared memory only when the number of columns are small enough. Our extension enables sparse-matrix sparse-vector multiplication by storing the vectors in sparse form when their degrees are small enough. We achieve full occupancy on the Volta architecture by trading off the size of the L1 cache to double the amount of shared memory per GPU, allowing each SM to use 96KiB. Since our design uses less than 32 registers, a block size of 32 warps allows two blocks, the full 64 warps, to be scheduled concurrently on each SM.

Input: $A_i, B, product_op, reduce_op$

Result: $C_{ij} = d(A_i, B_j)$

read A_i into shared memory;

$cur_row = rowidx[ind];$

$ind = idx$ of first elem to be processed by this thread;
 $c = product_op(A[ind], x[colidx[ind]]);$
for $i \leftarrow 1$ **to** nz_per_chunk ; **by** $warp_size$ **do**
 $next_row = cur_row + warp_size;$
 if $next_row \neq cur_row \parallel is_final_iter$ **then**
 $v = segmented_scan(cur_row, c, product_op);$
 if $is_segment_leader$ **then**
 | $atomic_reduce(v, reduce_op);$
 end
 $c = 0;$
 end
 $cur_row = next_row;$
 $ind += warp_size;$
 $c = product_op(A[ind], x[colidx[ind]]);$
end

Algorithm 3: Load-balanced Hybrid CSR+COO SPMV.

6.2.1 Two-pass execution. As described in subsection 4.2, a single execution of this strategy will compute the intersection and symmetric difference $\bar{a} \cap b$ between nonzero columns from each vector a , and b so long as \otimes is applied to all nonzero columns of b . While only a single pass covers distance measures which require only a column intersection (e.g. dot product semiring $(S, \mathbb{R}, \{+, 0\}, \{\ast, 1\})$), a second pass can compute the remaining symmetric difference required for the full union between non-zero columns by commuting A and B and skipping the application of id_{\otimes} in B for the second pass.

6.2.2 Sparsifying the Vector in Shared Memory. While we found storing the vectors from A in dense form in shared memory to have the highest throughput rate and least amount of thread divergence within each warp, sparse datasets are generally assumed to have high dimensionality and the limited amount of shared memory that can be allocated per SM bounds the size of the vectors that can be stored in it. For example, The 96KiB limit per block on Volta allows a max dimensionality of 23K with single-precision and the 163KiB limit per SM on Ampere allows a max dimensionality of 40K with single-precision. Coupling the amount of shared memory to the dimensionality creates a problem for occupancy as it approaches

capacity. Both of these architectures limit the maximum block sizes to 1024 threads and max concurrent warps per SM to 64 so anything over 48KB of shared memory per block is going to decrease occupancy. For this reason, the maximum dimensionality of dense vectors that can be processed with full occupancy is actually 12K and 20K, respectively.

This boundary becomes too small for many sparse datasets which would instead benefit from coupling the shared memory size to individual row degrees. Inspired by other sparse matrix multiplication implementations on the GPU [8, 30, 32, 34], we enhanced the vector insertion and lookup patterns of the COO SPMV design outlined in [2] by building a hash table to store these columns in shared memory. Unlike many other hash table implementations on the GPU [5, 6, 9, 13, 39], our implementation builds an independent hash table per thread-block and so many other designs and concurrency patterns that optimize the key distribution and collision-resolution strategies for the GPU are not efficient or cannot be easily ported for our use-case. For this reason, we used a simple hash table with a *Murmur* hash function and linear probing and leave the investigation of a better and more optimized design to future work.

Hash tables have the best performance when the number of entries is less than 50% of the capacity. As the hash table size grows beyond 50% capacity, the collision resolution cycles of linear probing, which are non-uniform, increase the serialization of instructions from warp divergences and also increase the number of transactions from global memory reads of B since they can no longer be coalesced. The hash table strategy decreases the amount of shared memory available, often by a factor of 2, because the nonzeros need to be stored together as key/value pairs to avoid an additional costly lookup to global memory, a side-effect which would only further increase serialized execution from diverging threads. Our hash table strategy allows for a max degree of 3K on Volta architectures and 5K on Ampere.

Another unfortunate side-effect from the linear-probing collision strategy of our hash table is the increase in lookup times for columns even for elements that aren't in the table. For example, as the hash table approaches capacity, the increase in collisions can cause a lookup to probe through multiple candidates, sometimes hundreds, before finding an element doesn't exist. Bloom filters have been used to implement fast list intersection problems for sparse matrix multiplication problems on the GPU [54, 55]. As an alternative to the hash table approach, we tried building a bloom filter in shared memory and used a binary search to perform lookups of nonzeros in global memory for positive hits. While we found this technique to yield marginally better performance on the Jensen-Shannon distance in one of our benchmarks, likely because it helped hide some of the compute-bound latencies from the additional arithmetic, we were not able to extract a simple rule from the data shapes or sparsity patterns that would allow us to know, before starting the computation, when it should be used.

6.2.3 Handling High Degree Columns. Our hash table implementation shows reasonable performance up to 50% capacity. Rows with degree greater than 50% hash table capacity are partitioned uniformly by their degrees into multiple blocks with subsets of the degrees that can fit into 50% hash table capacity. Using a similar

logic to that of blocked sparse techniques, our partitioning strategy does extra work in exchange for scale. Further, this technique requires each thread perform a branching conditional so it can test whether each nonzero column of B is part of the current partition. As we show in section 7, we do find that this strategy can perform well on some datasets when most of the degrees are small enough to fit in the hash table. For example, we found this strategy spent a minuscule amount of time in this step on the MovieLens dataset.

6.3 Norms and Expansion Functions

Distances which can be computed in their expanded forms can use the dot product semiring directly and only require a single pass through our SPSV. Computing distances in their expanded form often requires one or more arrays of row norms as well as an expansion function that can combine the norms with the individual dot products. It's fairly trivial to compute row norms over CSR formatted matrices as a row-wise reduction on the GPU as each row can be mapped to a single block or warp and the norm computed by a warp-level collective reduction.

The actual arithmetic in each expansion function is dependent upon the distance measure, however the kernel to apply the expansion function can be executed embarrassingly parallel by mapping each entry in the dot product matrix to an individual GPU thread to coalesce the reads and writes.

7 EXPERIMENTS

We evaluated the runtime performance characteristics and generalization of our approach by benchmarking our semiring strategies against several real-world sparse datasets with different shapes and degree distributions. We also analyze the GPU memory footprint of the cuSPARSE `csrgemm()` and our load-balanced COO SPMV.

7.1 Datasets

The datasets which we found are often used to benchmark sparse matrix-matrix and matrix-vector implementations on the GPU demonstrate the subtle differences in the objectives between using semirings for sparse neighborhood methods and using sparse linear algebra more generally for things like graph algorithms and eigen-decompositions. As an example, one such set of datasets which we found commonly used in papers to benchmark sparse linear algebra implementations [10, 50] is composed almost entirely of square connectivities graphs, and these would not provide a useful performance indicator for the objective of creating connectivities graphs from bipartite graphs. For this reason, and the lack of prior research in our objective, we establish a new baseline using datasets that our algorithm would be expected to encounter in practice. Our baseline uses cuSPARSE for all the expanded distance measures, along with the naive CSR full-union semiring implementation as described in section 6.1.2 for the distances which cuSPARSE does not support.

The *MovieLens* [25] Large dataset contains ratings given by 283k users for 194k movies. We used a dataset of 70k cells and gene expressions for 26k genes from the human cell atlas [48] as an example of a single-cell RNA workflow. For natural language processing examples, we benchmarked two different datasets containing TF-IDF vectors for two different use-cases. We used the NY Times

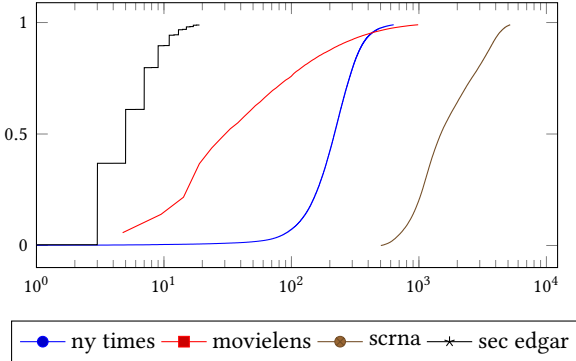


Figure 3: CDFs of Degree Distributions for the datasets used in our benchmark on the interval 0-99%. We can see that 99% of the degrees in the SEC Edgar datasets are <10 while 88% of the degrees for MovieLens are <200. On average scRNA has the largest degrees with 98% of the rows having degree 5k or less. The NY Times dataset has the highest variance, with 99% of the rows having degree less than 1k.

Bag of Words dataset[36] for an example of document similarity and n-grams generated from a list of company names from the SEC EDGAR company names database for an example of string matching.

Dataset	Size	Density	Min Deg	Max Deg
MovieLens Large	(283K, 194K)	0.05%	0	24K
SEC Edgar	(663K, 858K)	0.0007%	0	51
scRNA	(66K, 26K)	7%	501	9.6K
NY Times BoW	(300K, 102K)	0.2%	0	2K

Table 2: Datasets used in experiments

7.2 Runtime Performance

To get an idea of how each supported distance performed on data of different shapes and degree distributions, we benchmarked all of the supported distances for each of the datasets, even though some of them may provide irrelevant geometries in practice. Benchmarks were performed on a DGX1 containing dual 20-core Intel Xeon ES-2698 CPUs (80 total threads) at 2.20GHZ and a Volta V100 GPU running CUDA 11.0 for both the driver and toolkit. Each benchmark performs a k-nearest neighbors query to test our primitives end-to-end and allow scaling to datasets where the dense pairwise distance matrix may not otherwise fit in the memory of the GPU. We used Scikit-learn’s *NearestNeighbors* as a CPU baseline and configured it to use all the available CPU cores. Each experiment trains the *NearestNeighbors* estimator on the entire dataset and then queries the entire dataset, timing only the query. From the strategies described in Section 5, we benchmarked our best performing approach, the Load-balanced Hybrid COO+CSR SPMV described in subsection 6.2, using the hash table strategy to sparsify the vector in shared memory. The baseline implementation demonstrated very

high runtimes for many of the unexpanded distances so we allowed them to run for a max of 30min (1800s).

As evidenced in tables 3, 4, 5, and 6, our implementation consistently outperforms the CPU. We also outperform the baseline, cuSPARSE, for the distances that it supports in two out of the four datasets. In addition to maintaining comparable performance in the remaining two datasets, our design is also flexible enough to provide distances which require the semiring modifications outlined in subsection 4.2 while using less memory. As mentioned in section 2, it is not uncommon to see different sparse implementations performing better on some datasets than others [45] and the flexibility of our implementation, as well as our well-defined set of rules for supporting a wide array of distances, will allow us to continue optimizing our execution strategies to support patterns that we find frequently occurring across different sparse datasets.

7.3 Memory Footprint

The density of the dot product matrix that is returned from the cuSPARSE *csrgemm()* is fully dependent upon the dataset. Because 2 arrays, each of size nnz , are required to represent the cuSPARSE output in CSR format, a density of 50% would require the same amount of space as the full dense pairwise distance matrix. A density of 100% requires 2x the amount of space as the dense pairwise distance matrix. In addition, since the output still needs to be converted to a dense format, this requires an additional allocation of the dense pairwise distance matrix in a space of contiguous memory locations even if the cuSPARSE output was 99.9% dense. We found the density of the cuSPARSE output to be at least 57% on average across the batches for MovieLens, 98% for NY Times BoW and was fully dense in scRNA. The SEC Edgar datasets had the highest variance in density from batch-to-batch and were significantly different between n-gram sizes. The unigram and bigram dataset ranged from 5% to 25% output density, for example, while trigrams ranged from 24% to 43%.

This provides further evidence of the subtle but important differences between the types of data we expect to encounter in neighborhood methods, however even more evident is that the matrix resulting from computing the dot product semiring over the square connectivities graphs used in other sparse matrix multiplication research [10, 50] is extremely sparse. In addition to the output memory, cuSPARSE required an internal temporary workspace in device memory with anywhere from 300mb to 550mb of additional memory per batch while our dot product semiring required a workspace buffer of size $nnz(B)$ per batch. Strangely, the size of this temporary workspace seemed almost identical even when computed on the square connectivities graphs mentioned above.

8 CONCLUSION

In this paper, we demonstrated a flexible sparse pairwise distance primitive that is able to collectively support, to our knowledge, a larger assortment of widely-used distance measures than any other package on the GPU. We consolidated the design of these distance measures using a couple minor enhancements to the rules of classical semirings, which are traditionally used to implement graph algorithms, and we discussed the impact of our primitive

MovieLens			
Distance	CPU	Baseline	cuML
Correlation	X	130.57	111.20
Cosine	1733.30	131.39	110.01
Dice	X	130.52	110.94
Euclidean	1762.20	131.93	111.38
Hellinger	X	129.79	110.82
Jaccard	X	130.51	110.67
Russel-Rao	X	130.35	109.68
Canberra	X	1800.00	268.11
Chebyshev	X	1621.00	336.05
Hamming	X	1635.30	229.59
Jensen-Shannon	X	1800.00	415.12
KL Divergence	X	1800.00	170.06
Manhattan	2467.60	1632.05	227.98
Minkowski	X	1632.05	367.17

Table 3: Benchmark Results for movie ratings. All times are in seconds.

NY Times Bag of Words			
Distance	CPU	Baseline	cuML
Correlation	X	257.36	337.11
Cosine	2312.57	257.73	334.86
Dice	X	130.35	335.49
Euclidean	2083.04	258.38	336.63
Hellinger	X	258.22	334.80
Jaccard	X	258.24	336.01
Russel-Rao	X	257.58	332.93
Canberra	X	1800.00	819.80
Chebyshev	X	1800.00	1072.35
Hamming	X	1800.00	728.05
Jensen-Shannon	X	1800.00	1331.37
KL Divergence	X	1800.00	525.32
Manhattan	5072.90	1800.00	715.78
Minkowski	X	1800.00	1161.31

Table 5: Benchmark Results for document similarity. All times are in seconds.

scRNA			
Distance	CPU	Baseline	cuML
Correlation	X	207.00	235.00
Cosine	543.50	206.00	233.00
Dice	X	206.00	233.00
Euclidean	639.00	206.00	233.00
Hellinger	X	205.00	232.00
Jaccard	X	206.00	233.00
Russel-Rao	X	206.00	232.00
Canberra	X	1800.00	598.00
Chebyshev	X	1800.00	546.00
Hamming	X	1800.00	481.00
Jensen-Shannon	X	1800.00	1052.00
KL Divergence	X	1800.00	409.00
Manhattan	1552.00	1800.00	477.00
Minkowski	X	1800.00	838.00

Table 4: Benchmark Results for single-cell RNA. All times are in seconds.

SEC Edgar			
Distance	CPU	Baseline	cuML
Correlation	X	134.79	87.99
Cosine	5795.89	127.63	87.96
Dice	X	134.36	88.19
Euclidean	10058.10	134.75	87.77
Hellinger	X	134.11	87.83
Jaccard	X	134.55	87.73
Russel-Rao	X	134.31	87.94
Canberra	X	505.71	102.79
Chebyshev	X	253.00	146.41
Hamming	X	258.27	97.65
Jensen-Shannon	X	1248.83	142.96
KL Divergence	X	753.56	87.72
Manhattan	9559.93	254.69	98.05
Minkowski	X	646.71	129.47

Table 6: Benchmark Results for string matching. All times are in seconds.

as a core building block of many important neighborhood methods for machine learning and data mining. Finally, we provided a novel implementation as an example of how these semirings can be implemented on the GPU with a lower memory footprint and performance comparable to, or better than, the current state of the art.

REFERENCES

- [1] [n.d.]. GPU accelerated k-nearest neighbor kernel for sparse feature datasets. <https://repositories.lib.utexas.edu/handle/2152/65949>
- [2] 2020. Load-balancing Sparse Matrix Vector Product Kernels on GPUs. *ACM Transactions on Parallel Computing* 7, 1 (mar 2020). <https://doi.org/10.1145/3380930>
- [3] Martin Abadi, Paul Barham, Jianmin Chen, Zhifeng Chen, Andy Davis, Jeffrey Dean, Matthieu Devin, Sanjay Ghemawat, Geoffrey Irving, Michael Isard, et al. 2016. Tensorflow: A system for large-scale machine learning. In *12th {USENIX} symposium on operating systems design and implementation ({OSDI} 16)*. 265–283.
- [4] Akshay Agrawal, Alnur Ali, and Stephen Boyd. 2021. Minimum-Distortion Embedding. *arXiv preprint arXiv:2103.02559* (2021).
- [5] Dan A Alcantara, Andrei Sharf, Fatemeh Abbasinejad, Shubhabrata Sengupta, Michael Mitzenmacher, John D Owens, and Nina Amenta. 2009. Real-time parallel hashing on the GPU. In *ACM SIGGRAPH Asia 2009 papers*. 1–9.
- [6] Dan A Alcantara, Vasily Volkov, Shubhabrata Sengupta, Michael Mitzenmacher, John D Owens, and Nina Amenta. 2012. Building an efficient hash table on the GPU. In *GPU Computing Gems Jade Edition*. Elsevier, 39–53.
- [7] Daniel Alpay. 2012. *Reproducing kernel spaces and applications*. Vol. 143. Birkhäuser.
- [8] Pham Nguyen Quang Anh, Rui Fan, and Yonggang Wen. 2016. Balanced Hashing and Efficient GPU Sparse General Matrix-Matrix Multiplication.(2016), 1–12. *Google Scholar Google Scholar Digital Library Digital Library* (2016).
- [9] Saman Ashkiani, Martin Farach-Colton, and John D Owens. 2018. A dynamic hash table for the GPU. In *2018 IEEE International Parallel and Distributed Processing Symposium (IPDPS)*. IEEE, 419–429.

[10] Nathan Bell and Michael Garland. 2008. *Efficient sparse matrix-vector multiplication on CUDA*. Technical Report. Citeseer.

[11] Vaishak Belle and Luc De Raedt. 2020. Semiring programming: A semantic framework for generalized sum product problems. *International Journal of Approximate Reasoning* 126 (2020), 181–201.

[12] Alain Berlinet and Christine Thomas-Agnan. 2011. *Reproducing kernel Hilbert spaces in probability and statistics*. Springer Science & Business Media.

[13] Nathan Cassee and Anton Wijs. 2017. Analysing the performance of GPU hash tables for state space exploration. *arXiv preprint arXiv:1712.09494* (2017).

[14] Steven Dalton, Luke Olson, and Nathan Bell. 2015. Optimizing sparse matrix–matrix multiplication for the gpu. *ACM Transactions on Mathematical Software (TOMS)* 41, 4 (2015), 1–20.

[15] Timothy A Davis. 2018. *Algorithm 9xx: SuiteSparse:GraphBLAS: graph algorithms in the language of sparse linear algebra*. Technical Report. 24 pages.

[16] Timothy A Davis. 2019. Algorithm 1000: SuiteSparse: GraphBLAS: Graph algorithms in the language of sparse linear algebra. *ACM Transactions on Mathematical Software (TOMS)* 45, 4 (2019), 1–25.

[17] Jeffrey Dean and Sanjay Ghemawat. 2008. MapReduce: simplified data processing on large clusters. *Commun. ACM* 51, 1 (2008), 107–113.

[18] Christian Desrosiers and George Karypis. 2011. A comprehensive survey of neighborhood-based recommendation methods. *Recommender systems handbook* (2011), 107–144.

[19] Iain S Duff, Michael A Heroux, and Roldan Pozo. 2002. An overview of the sparse basic linear algebra subprograms: The new standard from the BLAS technical forum. *ACM Transactions on Mathematical Software (TOMS)* 28, 2 (2002), 239–267.

[20] Kento Emoto, Sebastian Fischer, and Zhenjiang Hu. 2012. Filter-embedding semiring fusion for programming with MapReduce. *Formal Aspects of Computing* 24, 4 (2012), 623–645.

[21] Alexandre Fender. 2017. *Parallel solutions for large-scale eigenvalue problems arising in graph analytics*. Ph.D. Dissertation. Université Paris-Saclay.

[22] Trevor Gale, Matei Zaharia, Cliff Young, and Erich Elsen. 2020. Sparse GPU kernels for deep learning. *arXiv preprint arXiv:2006.10901* (2020).

[23] Scott Gray, Alec Radford, and Diederik P Kingma. 2017. Gpu kernels for block-sparse weights. *arXiv preprint arXiv:1711.09224* 3 (2017).

[24] Cong Guo, Bo Yang Hsueh, Jingwen Leng, Yuxian Qiu, Yue Guan, Zehuan Wang, Xiaoying Jia, Xipeng Li, Minyu Guo, and Yuhao Zhu. 2020. Accelerating sparse dnn models without hardware-support via tile-wise sparsity. *arXiv preprint arXiv:2008.13006* (2020).

[25] F Maxwell Harper and Joseph A Konstan. 2015. The movielens datasets: History and context. *Acm transactions on interactive intelligent systems (tiis)* 5, 4 (2015), 1–19.

[26] Velimir M Ilic. 2011. Entropy semiring forward-backward algorithm for HMM entropy computation. *arXiv preprint arXiv:1108.0347* (2011).

[27] Michael Izbicki. 2013. Algebraic classifiers: a generic approach to fast cross-validation, online training, and parallel training. In *International Conference on Machine Learning*. PMLR, 648–656.

[28] Yongkweon Jeon, Baeseong Park, Se Jung Kwon, Byeongwook Kim, Jeongin Yun, and Dongsoo Lee. 2020. BiQGEMM: matrix multiplication with lookup table for binary-coding-based quantized DNNs. *arXiv preprint arXiv:2005.09904* (2020).

[29] Jeff Johnson and Facebook AI Research Paris HervéHerv. [n.d.]. *Billion-scale similarity search with GPUs Matthijs Douze*. Technical Report. arXiv:1702.08734v1 <https://github.com/facebookresearch/faiss>

[30] Rakshith Kunchum. 2017. *On improving sparse matrix-matrix multiplication on gpus*. Ph.D. Dissertation. The Ohio State University.

[31] Neil D Lawrence and Raquel Urtasun. 2009. Non-linear matrix factorization with Gaussian processes. In *Proceedings of the 26th annual international conference on machine learning*, 601–608.

[32] Weifeng Liu and Brian Vinter. 2014. An efficient GPU general sparse matrix–matrix multiplication for irregular data. In *2014 IEEE 28th International Parallel and Distributed Processing Symposium*. IEEE, 370–381.

[33] Tim Mattson, David Bader, Jon Berry, Aydin Buluc, Jack Dongarra, Christos Faloutsos, John Feo, John Gilbert, Joseph Gonzalez, Bruce Hendrickson, et al. 2013. Standards for graph algorithm primitives. In *2013 IEEE High Performance Extreme Computing Conference (HPEC)*. IEEE, 1–2.

[34] Yusuke Nagasaka, Akira Nukada, and Satoshi Matsuoka. 2017. High-performance and memory-saving sparse general matrix–matrix multiplication for nvidia pascal gpu. In *2017 46th International Conference on Parallel Processing (ICPP)*. IEEE, 101–110.

[35] M Naumov, LS Chien, P Vandermersch, and U Kapasi. 2010. Cusparse library. In *GPU Technology Conference*.

[36] David Newman. 2008. UCI Machine Learning Repository. <http://archive.ics.uci.edu/ml>

[37] Corey J Nolet, Victor Lafargue, Edward Raff, Thejaswi Nanditale, Tim Oates, John Zedlewski, and Joshua Patterson. 2020. Bringing UMAP Closer to the Speed of Light with GPU Acceleration. *arXiv preprint arXiv:2008.00325* (2020).

[38] Amra Omanović, Hilal Kazan, Polona Oblak, and Tomaž Curk. 2020. Data embedding and prediction by sparse tropical matrix factorization. *arXiv:2012.05210 [cs.LG]*

[39] Jia Pan and Dinesh Manocha. 2011. Fast GPU-based locality sensitive hashing for k-nearest neighbor computation. In *Proceedings of the 19th ACM SIGSPATIAL international conference on advances in geographic information systems*. 211–220.

[40] Adam Paszke, Sam Gross, Francisco Massa, Adam Lerer, James Bradbury, Gregory Chanan, Trevor Killeen, Zeming Lin, Natalia Gimelshein, Luca Antiga, et al. 2019. Pytorch: An imperative style, high-performance deep learning library. *arXiv preprint arXiv:1912.01703* (2019).

[41] Sebastian Raschka, Joshua Patterson, and Corey Nolet. 2020. Machine learning in python: Main developments and technology trends in data science, machine learning, and artificial intelligence. *Information* 11, 4 (2020), 193.

[42] JS Ratti and YF Lin. 1971. The graphs of semirings. II. *Proc. Amer. Math. Soc.* 30, 3 (1971), 473–478.

[43] Bernhard Schölkopf, Ralf Herbrich, and Alex J Smola. 2001. A generalized representer theorem. In *International conference on computational learning theory*. Springer, 416–426.

[44] Bernhard Schölkopf and Alexander J Smola. 2018. *Learning with kernels: support vector machines, regularization, optimization, and beyond*. Adaptive Computation and Machine Learning series.

[45] Naser Sedaghati, Arash Ashari, Louis-Noël Pouchet, Srinivasan Parthasarathy, and P Sadayappan. 2015. Characterizing dataset dependence for sparse matrix–vector multiplication on GPUs. In *Proceedings of the 2nd workshop on parallel programming for analytics applications*. 17–24.

[46] Alex Smola, Arthur Gretton, Le Song, and Bernhard Schölkopf. 2007. A Hilbert space embedding for distributions. In *International Conference on Algorithmic Learning Theory*. Springer, 13–31.

[47] Nvidia Tesla. 2018. V100 GPU architecture. *Online verfügbar unter <http://images.nvidia.com/content/volta-architecture/pdf/volta-architecture-whitepaper.pdf>, zuletzt geprüft am 21 (2018)*.

[48] Kyl J Travaglini, Ahmad N Nabhan, Lolita Penland, Rahul Sinha, Astrid Gillich, Rene V Sit, Stephen Chang, Stephanie D Conley, Yasuo Mori, Jun Seita, et al. 2020. A molecular cell atlas of the human lung from single-cell RNA sequencing. *Nature* 587, 7835 (2020), 619–625.

[49] Michael Wachter, Rolf Haenni, and Marc Pouly. 2007. Optimizing inference in Bayesian networks and semiring valuation algebras. In *Mexican International Conference on Artificial Intelligence*. Springer, 236–247.

[50] Samuel Williams, Leonid Oliker, Richard Vuduc, John Shalf, Katherine Yellick, and James Demmel. 2007. Optimization of sparse matrix–vector multiplication on emerging multicore platforms. In *SC’07: Proceedings of the 2007 ACM/IEEE Conference on Supercomputing*. IEEE, 1–12.

[51] Carl Yang, Aydin Buluc, and John D Owens. 2018. Design principles for sparse matrix multiplication on the gpu. In *European Conference on Parallel Processing*. Springer, 672–687.

[52] Carl Yang, Aydin Buluc, and John D Owens. 2019. GraphBLAST: A high-performance linear algebra-based graph framework on the GPU. *arXiv preprint arXiv:1908.01407* (2019).

[53] Orestis Zachariadis, Nitin Satpute, Juan Gómez-Luna, and Joaquín Olivares. 2020. Accelerating sparse matrix–matrix multiplication with GPU Tensor Cores. *Computers & Electrical Engineering* 88 (2020), 106848.

[54] Fan Zhang, Di Wu, Naiyong Ao, Gang Wang, Xiaoguang Liu, and Jing Liu. 2011. Fast lists intersection with bloom filter using graphics processing units. In *Proceedings of the 2011 ACM Symposium on Applied Computing*. 825–826.

[55] Zhekai Zhang, Hanrui Wang, Song Han, and William J Dally. 2020. Sparc: Efficient architecture for sparse matrix multiplication. In *2020 IEEE International Symposium on High Performance Computer Architecture (HPCA)*. IEEE, 261–274.

[56] Brady Beida Zhou. 2018. *GPU accelerated k-nearest neighbor kernel for sparse feature datasets*. Ph.D. Dissertation.